EES Batteries

PAPER

View Article Online
View Journal | View Issue

Cite this: *EES Batteries*, 2025, **1**, 310

Induced orbital asymmetry of nonpolar molecular additives for boosted rapid operating performance in lithium metal batteries†

Seo-Young Jun,[a] Chae Yeong Son,[a] Suji Kim,[a] Haesun Park[b] and Won-Hee Ryu *[a,c]

Lithium metal batteries (LMBs) have emerged as a promising next-generation energy storage solution owing to their high energy density; however, the uncontrolled growth and short circuits of lithium dendrites on lithium metal anodes result in short lifespans and severe safety concerns. In this study, we introduced highly polarizable and nonpolar molecular additives into the electrolyte to stabilize the lithium metal anode surface, emphasizing the role of the induced dipole effects in these molecules. Specifically, we compared the effects of benzene and anthracene additives, both nonpolar molecules with different polarizabilities, on the performance of LMBs. Our findings reveal that larger and more polarizable anthracene molecules flatten the lithium metal surface and significantly enhance the cycling stability under high current densities, even up to 10 mA cm^{-2}. The crystalline orientation of lithium metal was controlled along the planar (110) direction, and a durable solid electrolyte interface layer was formed owing to the active surface coordination of the highly polarizable anthracene. This study underscores the pivotal influence of molecular polarizability in guiding the design of electrolyte additives. It paves the way for developing long-lasting and high-performance LMBs.

Received 5th February 2025,
Accepted 28th February 2025

DOI: 10.1039/d5eb00021a

rsc.li/EESBatteries

Broader context

The advancement of lithium metal batteries (LMBs) holds great promise for next-generation energy storage, offering significantly higher energy density compared to conventional lithium-ion batteries. However, the practical deployment of LMBs is hindered by critical issues such as uncontrolled lithium dendrite growth, unstable solid electrolyte interface (SEI) formation, and rapid capacity degradation. Recent research has focused on electrolyte engineering as a viable strategy to enhance lithium metal anode stability. In this study, we introduce a novel approach utilizing highly polarizable nonpolar molecular additives to suppress dendritic lithium growth and improve cycling stability under high current densities. By investigating benzene and anthracene as model additives, we demonstrate that higher molecular polarizability enhances surface leveling effects, stabilizes lithium deposition, and promotes a durable SEI layer. This work highlights the critical role of molecular polarizability in electrolyte design, independent of intrinsic dipole moments, offering new insights into electrolyte additive development for high-performance and long-lasting LMBs. Our findings provide a foundation for future studies on molecular-level electrolyte optimization, paving the way for safer and more efficient lithium-based energy storage systems.

1. Introduction

To surpass the performance limitation of existing lithium-ion batteries (LIBs), diverse alternatives of next-generation batteries emerging from low-capacity anode parts have been explored.[1–9] Lithium metal batteries (LMBs) are a game changer battery technology, leveraging the exceptionally high theoretical capacity of lithium metal (3860 mA h g^{-1}), low density (0.59 g cm^{-3}), and the lowest electrochemical redox potential (−3.04 V *vs.* the standard hydrogen electrode,

[a]*Department of Chemical and Biological Engineering, Sookmyung Women's University, 100 Cheongpa-ro 47-gil, Yongsan-gu, Seoul 04310, Republic of Korea. E-mail: whryu@sookmyung.ac.kr*
[b]*School of Integrative Engineering, Chung-Ang University, 84, Heukseok-ro, Dongjak-gu, Seoul, 06974, Republic of Korea*
[c]*Institute of Advanced Materials and Systems, Sookmyung Women's University, 100 Cheongpa-ro 47-gil, Yongsan-gu, Seoul 04310, Republic of Korea*
† Electronic supplementary information (ESI) available. See DOI: https://doi.org/10.1039/d5eb00021a

SHE).[2,3,10,11] Although the LMBs can offer exceptional energy density merit, the Li metal anode intrinsically suffers from problematic dendritic growth of Li, causing short-circuit and consequent safety concerns.[2,12–14] Moreover, dendrite residues detached during cycling result in the accumulation of 'dead Li', diminishing the coulombic efficiency and causing excessive surface resistance.[2,15,16] Lastly, the continuous formation of the solid electrolyte interface (SEI) layer on the Li metal by electrolyte decomposition leads to vigorous volume change and electrolyte depletion, thereby deteriorating battery lifespan.[2,3,14,17,18] To address the interface issues, various strategies have been reported such as utilization of 3-D host structure, separator modifications,[19–23] formation of artificial SEI layer,[18,24–26] and introduction of electrolyte additive.[10,11,27–31]

Attempts have been made to regulate the SEI layer components with durable species by employing electrolyte additives such as vinylene carbonate (VC) and fluoroethylene carbonate (FEC). Nevertheless, most electrolyte additives do not properly control the morphological and structural growth mechanisms of Li, except for SEI modification. Our group recently proposed pyrrolidone-based molecular dipoles as effective electrolyte additives derived from leveling additives for conventional electroplating techniques, enabling the surface flattening of Li metal anodes.[10,11,32] Molecular dipole electrolyte additives for LMBs offer the following trifunctional advantages: (i) flattening of the Li surface for repeated Li deposition and stripping, (ii) control of the growth mechanism of crystalline Li along the lateral direction and (iii) reinforcement of the SEI layer by durable fluoride and carbonate species. The permanent dipole moment originating from the asymmetric structure of the pyrrolidone molecules can help selectively adsorb the defect sites and consequently enable surface energy equality, thereby achieving surface leveling of the Li metal surface instead of the dendritic growth of Li. Recently, it was also reported that the larger polarizability factor of the molecular additives, proportional to the molecular volume, further distorts the orbital structure under a highly applied field and boosts the adsorption ability on the Li defect sites.[32] In this regard, the cycle performance of Li metal anodes can be significantly improved up to 600 cycles, even under an extremely high current density of over 5 mA cm^{-2}, corresponding to fast charging operation, by introducing highly polarizable and larger molecular dipole additives compared to relatively low polarizability and smaller additives. Advanced and elaborate approaches show the efficacy and significance of polarizability engineering; however, the proposed concept regarding the polarizability factor should be further verified for optimizing the electrolyte additive. Because the permanent dipole moment of the intrinsically polar molecule geometry can be simultaneously affected by adsorption and interaction behavior at the Li electrode/electrolyte interface in the previous study, further studies independent of the permanent dipole moment are needed to verify the function of the induced dipole moment as a function of molecular polarizability for tailoring surface-stabilizing electrolyte agents.

In this study, we prove the importance of polarizability control by comparing "nonpolar" molecular electrolyte additives with different molar volumes and corresponding polarizabilities for long and rapid-operating LMBs (Fig. 1). Benzene (C_6H_6) and anthracene ($C_{14}H_{10}$) were chosen as symmetric and nonpolar molecules, respectively (electric dipole moment: 0 D). We investigated the surface smoothing effects achievable by introducing nonpolar molecule additives under various electrical field conditions, ranging from low current density of 1 mA cm^{-2} to high current density of 10 mA cm^{-2}. We confirmed the outstanding lifespan improvement capabilities of the highly polarizable nonpolar additives under rapid operating conditions. We also conducted *in situ* electrochemical impedance spectroscopy (EIS) studies on the Li symmetric cells employing different nonpolar molecules to investigate the change in charge transfer resistance at the Li electrode/electrolyte interface. The surface flattening effects accelerated by the distorted orbital asymmetry of nonpolar molecular additives under a highly applied field were confirmed through diverse morphological observations and surface roughness analyses. We examined the preferred nucleation and growth of the deposited Li metal along a direction parallel to the crystalline arrangement. Furthermore, chemical reinforcement of the SEI component was demonstrated after the self-reduction and decomposition of the molecular additives originating from their unique electron-donating conjugated structure. We propose key strategies for realizing high-energy Li metal battery systems, emphasizing the significant effects of molecular polarizability on the morphological and structural changes in Li metal anodes during repeated cycling, especially under high-current-density conditions. This provides a potential key to developing advanced electrolyte additives that promote the safety and long-cycle performance of LMBs.

2. Results and discussion

2.1. Nonpolar molecule-induced polarizability: a novel mechanism for Li–metal anode stabilization

Based on previous studies, we hypothesize that the geometric orbital distortion generating an induced dipole moment is dominant in stabilizing Li–metal anodes, especially under highly applied fields related to fast charging and discharging operations. We investigated the independent polarizability effect, regardless of the permanent dipole moment variable, on stabilizing a lithium metal anode by introducing nonpolar molecules. By controlling the number of benzene rings, we chose benzene and anthracene molecules with different sizes of nonpolar molecules. Computational calculations were performed to understand better the molecular properties of monocyclic benzene and tricyclic anthracene, as shown in Fig. 1. Both benzene and anthracene molecules used as additives were confirmed to be symmetric and nonpolar structures with a dipole moment value of 0 D. However, the molecules exhibited different molecular sizes, measuring 88.9 and 143.3 cm^3 mol^{-1}, respectively. Consequently, a notable differ-

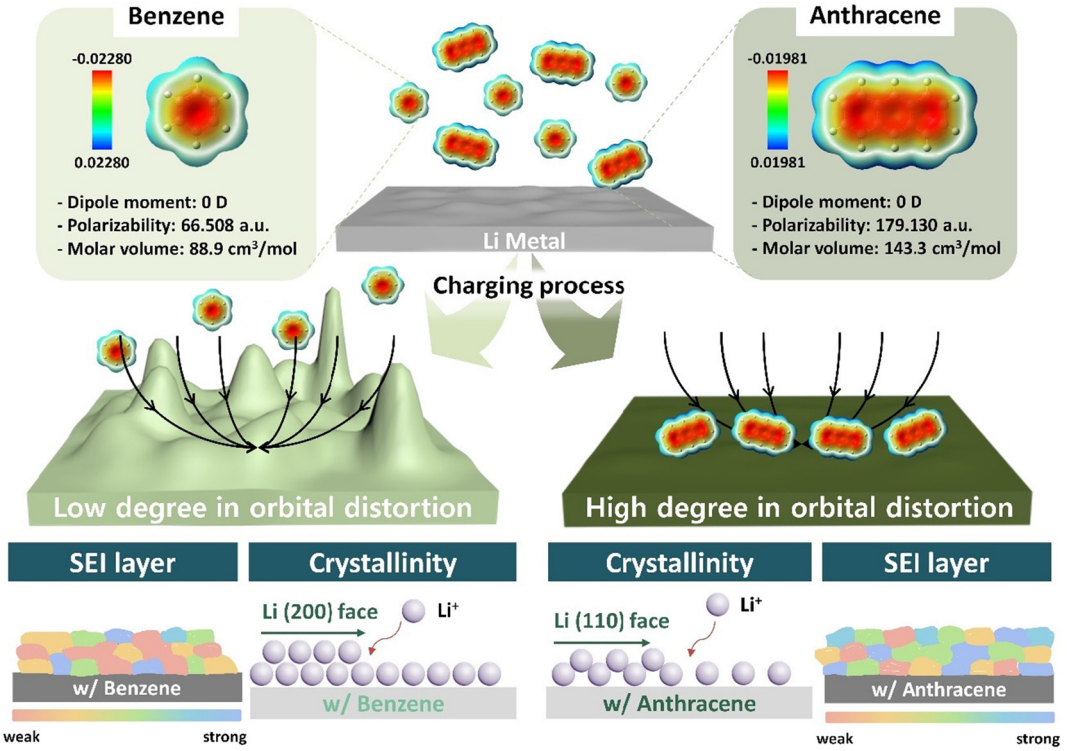

Fig. 1 Schematic illustration of the multifunctional effects of nonpolar additives in lithium metal anode.

ence in the polarizability values resulting from the intramolecular electron distribution was observed between the two molecules. The calculated polarizability values were 66.508 a.u. for benzene and 179.130 a.u. for anthracene. Although the molecular volumes of the two additives differed by approximately 2-fold, the polarizability values of anthracene corresponding to intramolecular electron delocalization were approximately 3-fold higher than those of benzene, implying facile orbital distortion by the external electric field. This computational validation emphasizes that even for nonpolar molecules with the same 0 D dipole moment, there is a substantial difference in polarizability values based on molecular size. Calculations also confirmed that the dipole moment of the molecules present in an electric field increased proportionally as the electric field increased (Fig. S1†). When the electric field is 0 eV $Å^{-1}$, the dipole moments of both benzene and anthracene are 0.000 D. However, as the electric field increases to 0.06 eV $Å^{-1}$, the dipole moments of benzene and anthracene continuously increase to 0.131 and 0.252 D, respectively. At this point, the magnitude of the increase in the dipole moment, similar to the polarizability value, became more significant as the molecular size increased. Fig. 1 shows the electrostatic potential maps, dipole moments, polarizabilities, and molecular volumes of the two molecules. The computational results lay the groundwork for investigating the lifespan of Li–Li symmetric cells, considering the changes in polarizability characteristics upon introducing nonpolar molecule additives. The enhanced electron delocalization originating from the larger polarizability of anthracene compared to that of benzene becomes more pronounced under the applied electric field during charging. This creates an environment in which the additive molecules, despite their nonpolar nature, effectively interact with the positively or negatively charged surface of the Li metal anode.

2.2. Electrochemical performance of Li–Li symmetric cells with nonpolar additives

Electrochemical Li–Li symmetric cell tests were conducted to directly validate our hypothesis that non-polar additives with high polarizability stabilize Li metal anodes. In the Li–Li symmetric cell experiments, various indicators related to the degradation of the Li metal anode were observed. As the cell operates, issues such as excessive electrolyte consumption, formation of the SEI layer at the interface, dendrite growth, and dead Li formation collectively contribute to an increase in overpotential, voltage fluctuation, or a sudden voltage drop, leading to short circuits.[2,33] In this study, the criteria for determining cell degradation over time were established based on the increasing overpotential, with a threshold of 1 V. Fig. 2a–c present the results of Li–Li symmetric cell tests conducted under different current density conditions (1, 5, and 10 mA cm^{-2}) with a consistent capacity limit of 1 mA h cm^{-2}. Higher current density, even at 10 mA cm^{-2}, induces significant orbital distortion and strong adsorption of the nonpolar additives on Li metal anode. Under a current density of 1 mA cm^{-2}, the cycling lifetimes were 146 h for the cell without additives, 135 h for the cell with benzene, and 259 h for the cell with anthracene (Fig. 2a). Although anthracene showed somewhat

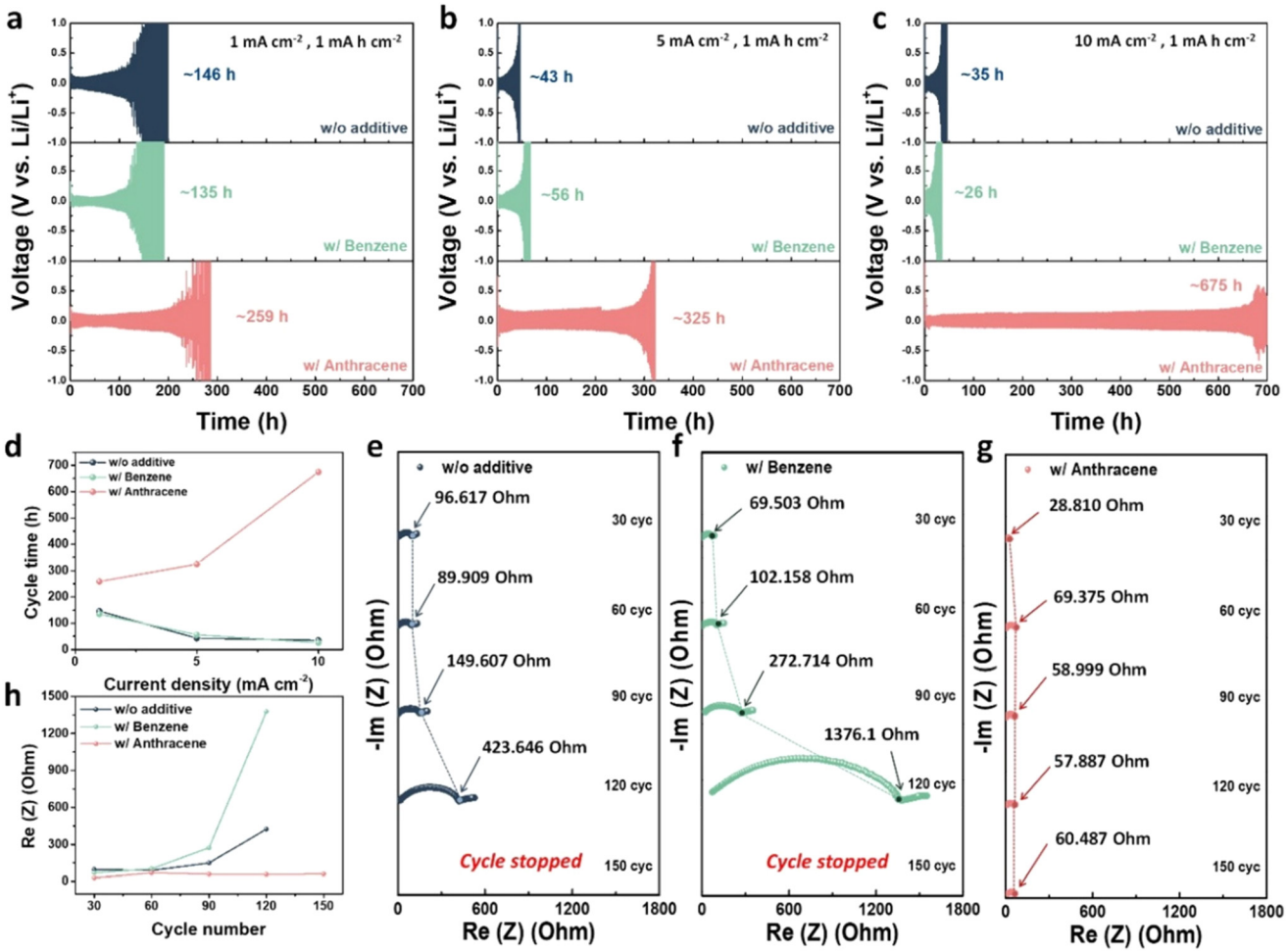

Fig. 2 (a) Cycling performance of the Li–Li symmetric cell without additive and with nonpolar additives (benzene and anthracene) at a low current density of 1 mA cm^{-2}, (b) at a middle current density of 5 mA cm^{-2}, and (c) at a high current density of 10 mA cm^{-2}. (d) Cycle time data illustrating the additive effects conducted at different current densities. (e) EIS spectra obtained from the Li–Li symmetric cells using the pristine electrolyte, (f) electrolyte with benzene, and (g) electrolyte with anthracene at different cycle numbers.

improved cycling properties, no significant difference in the stabilization of non-polar molecules was observed under low electric field conditions. However, when the experiments were conducted under gradually increasing current densities of 5 and 10 mA cm^{-2}, extended lifetime characteristics were observed for benzene (low polarizability) and anthracene (high polarizability). At 5 mA cm^{-2}, the lifetimes of the Li–Li symmetric cell without additives and with benzene were 43 and 56 h, respectively. However, the lifetime of the cell with anthracene significantly improved to 325 h, surpassing the results obtained under low-current-density conditions (Fig. 2b). This trend became more apparent when the current density increased to 10 mA cm^{-2}. The Li–Li symmetric cells without additives and with benzene showed shorter lifetimes of 35 and 26 h, respectively. By contrast, the cell with anthracene delivered a notably stable cycle for up to 675 h without a significant overpotential (Fig. 2c). Generally, in situations where lithium deposition and stripping proceed rapidly, such as high current densities, further severe side reactions, including dendrite growth and surface instability, occur, resulting in huge overpotentials and short-circuit issues of the LMBs. Therefore, as expected, the cycle performance of cells without additives and with benzene rapidly deteriorated with increasing current density. Contrary to expectations, introducing anthracene as a highly polarizable additive resulted in exceptional cycling behavior, achieving at least a 20-fold longer performance even at a high current density of 10 mA cm^{-2}. Fig. 2d summarizes the significant differences in the lifetime characteristics when employing different polarizable non-polar additives at various current densities. The significant effect of the highly polarizable, nonpolar anthracene molecule strongly demonstrates that the induced electron localization in these molecules promotes stronger adsorption on defects or protruding sites where localized electric fields appear. This, in turn, prevents dendritic growth of Li and results in a smoother surface. Consistent with the results of our previous study, the introduction of molecular dipoles as electrolyte additives improved the cycling performance of Li metal anodes at higher current den-

sities as the polarizability values increased. Given our results with nonpolar additives, it is evident that polarizability is the dominant factor in stabilizing Li metal anodes, particularly under rapid operating conditions.

To investigate the interfacial resistance of the Li metal anode with the electrolyte or SEI layer, *in situ* electrochemical impedance spectroscopy (EIS) analyses were performed using Li–Li symmetric cells (Fig. 2e–h). *In situ* EIS was used to determine the resistance (R_{sol}) arising from the movement of Li ions across the interface of the electrolyte, separator, and Li metal electrode. It also assesses the charge transfer resistance (R_{ct}) associated with Li-ion diffusion between the electrolyte/SEI layer and between the SEI layer/Li metal electrode.[34–37] R_{sol}, which is most influenced by the electrolyte, is commonly used to indicate electrolyte degradation.[34,35,37] Typically, as the cycling process progresses, side reactions such as electrolyte decomposition often hinder the movement of Li ions, resulting in a decrease in Li-ion conductivity and an increase in R_{sol}. Concurrently, R_{ct} at the electrode–electrolyte interface increases during electrochemical reactions. Fig. 2e–g presents the interfacial resistance of the Li–Li symmetric cell measured every 30 cycles using electrolytes with and without additives (benzene and anthracene). The Li–Li cell without additives and with benzene showed a continuous increase in the R_{ct} value corresponding to the diameter of the semicircle, and their cell operation eventually stopped after 120 cycles due to interface deterioration. In the cell with benzene, the increase in resistance became more severe than that in the pristine cell because the adsorbed and decomposed benzene molecules accelerated interfacial degradation on the Li metal rather than providing a surface-stabilizing function. Furthermore, the cell employing anthracene operated stably for up to 150 cycles and consistently maintained interfacial resistance without a significant increase. Fig. 2h shows the overall resistance values over the cycles when using a pristine electrolyte and an electrolyte containing a nonpolar additive. The Li–Li symmetric cell deteriorates further with the addition of benzene molecules, indicating that the incorrect selection of additives adversely affects cell performance. The stable interface reaction behavior of the cell utilizing anthracene molecules suggests that increasing the polarizability of nonpolar molecules is crucial to achieving longer cycling properties of LMBs, even under fast operation conditions.

2.3. Surface morphology evolution of Li metal anodes with nonpolar additives

To further explore the surface flattening and interfacial stabilization effects arising from the differences in the polarizability of nonpolar additives, we conducted a surface morphology analysis using *ex situ* scanning electron microscopy (SEM). The *ex situ* SEM analysis was performed after 100 cycles at a current density of 5 mA cm^{-2}, introducing various nonpolar molecule additives (Fig. 3). Fig. 3a and d depict the surface of the reacted Li metal anode using an electrolyte without addi-

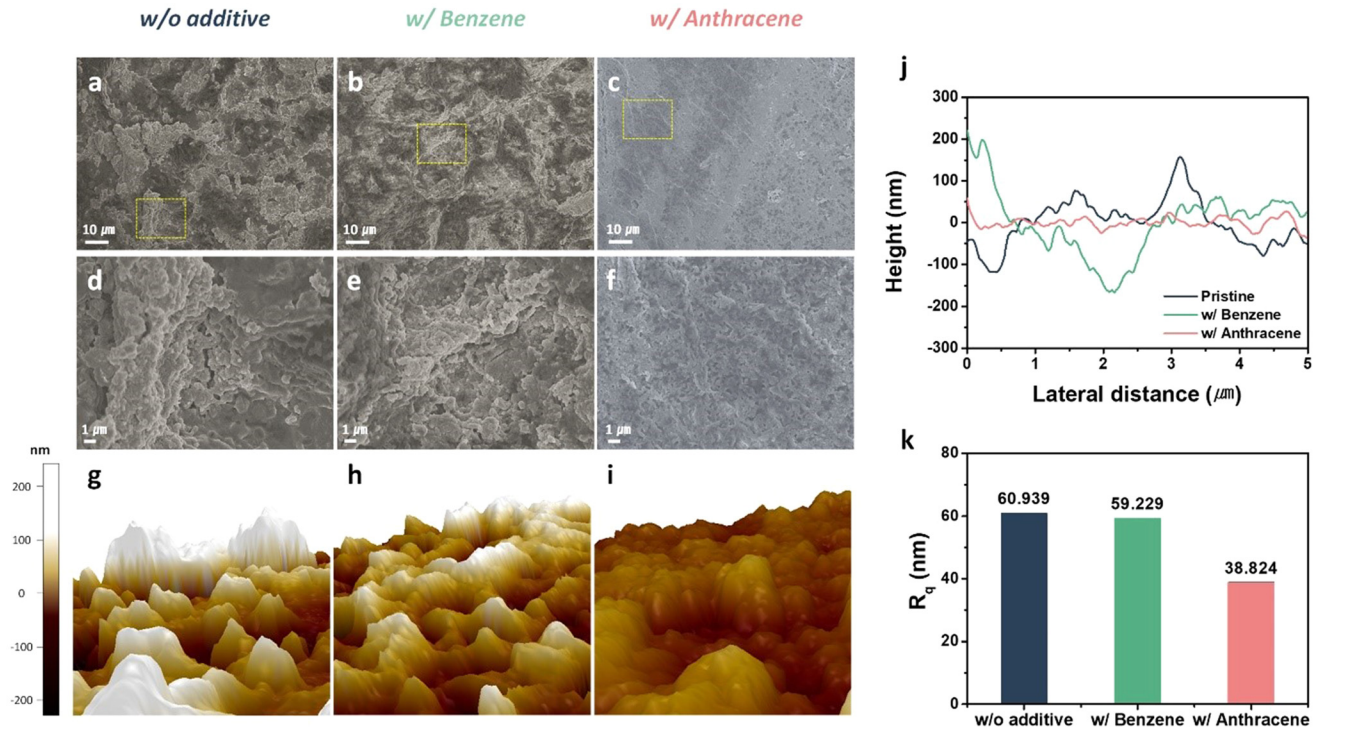

Fig. 3 *Ex situ* surface analysis of Li–Li symmetric cells that form differently depending on electrolyte additives. SEM images of the Li–metal after 100 cycles at a current density of 5 mA cm^{-2} in the electrolyte (a) without additive, (b) with benzene, and (c) with anthracene. (d)–(f) Enlarged SEM images of (a), (b), and (c) respectively. AFM images of the Li–metal morphology in the electrolyte (g) without additive, (h) with benzene, and (i) with anthracene. (j) Cross-sectional height and (k) surface roughness values from the AFM analysis.

tives. As expected, irregular and bumpy surfaces were observed owing to the dendritic formation of Li and excessive accumulation of side products during charging and discharging. Fig. 3b and e show SEM images after cycling in the presence of benzene. Nodules and irregular surface features of the Li metal anode are also observed, similar to those of the pristine electrolyte without additives. Consistent with the electrochemical data, it is evident that the surface stabilization effect is minimal when benzene, characterized by its low polarizability, is introduced. However, when anthracene molecules with high polarizability were introduced as additives, a smooth and planar surface of the Li metal anode was observed, even after prolonged cycling, verifying their effective surface flattening effect (Fig. 3c and f).

We used *ex situ* atomic force microscopy (AFM) to quantitatively evaluate the surface roughness and cross-sectional height of the Li metal electrode after 100 cycles with and without additives. Fig. S2† shows digital images of the surface of the Li metal anode after 100 cycles. These images reveal that in cases where electrolytes without additives and less polarizable benzene were used, a significantly darkened black surface was observed due to side reactions. In agreement with the SEM results, the Li metal electrodes cycled without additives and with benzene exhibited rough and uneven surfaces owing to nonuniform lithium deposition (Fig. 3g and h and S3a and S3b†). Conversely, the Li electrode cycled with the highly polarizable anthracene displayed a uniform and smooth surface with fresh Na, indicating uniform Li plating and stripping without significant side reactions (Fig. 3i and S3c†). The analysis results of the vertical cross-sectional height of the Li metal electrode obtained after cycling are shown in Fig. 3j. In cases where the Li anode cycled without additives and with benzene, the surface roughness of the Li metal electrode after cycling showed apparent deviation and variation. By contrast, the Li metal electrode cycled with anthracene exhibits a uniform height profile without significant surface curvature. Higher surface roughness values were observed for the Li metal electrodes cycled without additives (60.939 nm) and with benzene (59.229 nm). However, a significantly decreased surface roughness (38.824 nm) was achieved by introducing anthracene (Fig. 3k). From the morphological investigation, we directly elucidated the surface leveling effects of highly polarizable nonpolar molecules.

2.4. Crystalline rearrangement dynamics of Li metal anodes with nonpolar additives

To further investigate the atomic nucleation and growth behavior of the Li metal anode, resulting in crystalline rearrangement during cycling, *ex situ* X-ray diffraction (XRD) analysis was conducted on the cycled electrodes in different electrolytes. In a stable and uniform charging and discharging process, the crystalline Li metal forms a close-packed structure, represented by a body-centered cubic (bcc) structure, as shown in Fig. 4a. However, when additives are not included, and the surface crystallinity cannot be controlled, repeated charging and discharging cycles can destroy the crystallinity of Li, leading to the formation of dead Li and dendritic growth. Additionally, this process generates a large number of side products, further contributing to the breakdown of Li metal crystallinity. However, the crystallinity was maintained when benzene was used as an additive, but dendritic growth was observed on the (200) plane. Conversely, when anthracene, which has a larger molecular size and higher polarizability, was used as an additive, the Li metal grew smoothly along the (110) plane even after high-speed charging and discharging. Moreover, previous research findings suggest that the crystalline orientation of the (110) plane formed by the Li metal anode induces low overpotential, contributing to the formation of a stable Li metal anode.[38,39] To assess the surface crystallinity of Li metal after 100 charge and discharge cycles under two different current densities, 5 and 10 mA cm^{-2}, data related to the direction of crystalline growth were examined. The crystallinity was poorly maintained without additives after 100 charge and discharge cycles. Compared to the other two samples, the intensity significantly decreased and nearly disappeared (Fig. 4b–d). This observation suggests that the crystallinity of the Li metal was lost, resulting from unwanted side reactions such as a thick SEI layer and dead Li formation, as shown in Fig. 4e and f. By contrast, when benzene and anthracene were introduced, the crystallinity intensity was well-maintained even after prolonged charge and discharge cycles (Fig. 4e and f). However, the two additives exhibit different crystalline orientations. With the introduction of benzene, a relatively vertical growth of the crystallinity towards the (200) plane was induced. By contrast, anthracene induces horizontal growth towards the (110) plane (Fig. 4e and f). Although both additives maintained their crystallinity under different conditions, the introduction of anthracene with significant polarizability suggested a beneficial rearrangement effect in promoting the parallel direction of Li plating and stripping on the surface of the Li metal anode.

2.5. Molecular additive effects on solid electrolyte interface formation

During the first charging process of the battery full cell, a solid electrolyte interface (SEI) layer is formed on the anode surface. The SEI layer is primarily formed through the reduction and decomposition reactions of the electrolyte species. When an electrolyte containing appropriate additives is used, the additive molecules preferentially undergo reduction and decomposition before the solvent molecules in the electrolyte, consequently influencing the primary composition of the SEI layer. A crucial consideration in this process is the relative energy levels of the additive molecules and electrolyte solvent, which determine the dominance of the decomposition reaction derived from the diverse species for SEI formation. Energy level calculations were performed to identify the highest occupied molecular orbital (HOMO) and lowest unoccupied molecular orbital (LUMO) energy levels of the nonpolar additives and TEGDME solvent (Fig. 5a). The calculation results confirmed that benzene and anthracene had lower LUMO energy levels than the electrolyte solvent, TEGDME, indicating that

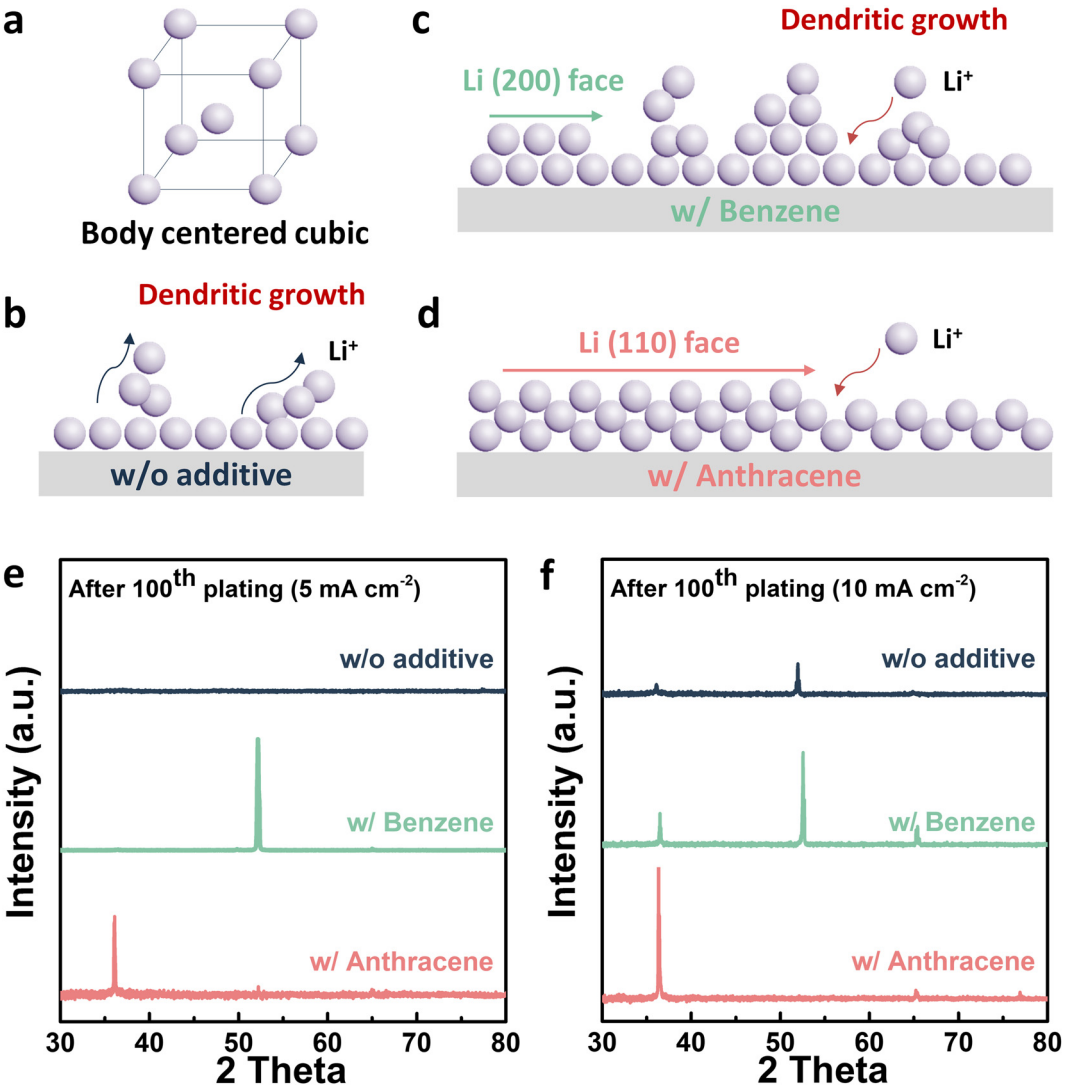

Fig. 4 (a) Structural representation showing typical crystalline state of lithium metal. (b) Schematic illustrating the crystalline orientation of the lithium metal anode surface after prolonged charging and discharging using electrolyte without additives, (c) with the inclusion of benzene as an additive, and (d) with anthracene as an additive. *Ex situ* X-ray diffraction (XRD) peaks of the lithium metal electrode obtained (e) after 100th plating at the current density of 5 mA cm^{-2}, and (f) after 100th plating at the current density of 10 mA cm^{-2} with and without additives.

the predominant reduction and subsequent decomposition of the benzene and anthracene molecules occurred before the TEGDME solvent. This implies an impact on the chemical composition change of the SEI layer and an inhibitory effect on unnecessary electrolyte decomposition during cell operation.

We conducted *ex situ* X-ray photoelectron spectroscopy (XPS) measurements on the Li metal anodes after cycling using different electrolytes to analyze further the composition and interfacial structure of the SEI layer (Fig. 5c–f). Distinct C 1s spectrum, distinct C–H and C–O peaks corresponding to the decomposition reaction products of the TEGDME electrolyte are observed under all conditions (Fig. 5c). Although only in trace amounts, the introduction of anthracene as an additive led to the observation of CF_3 peaks in the fluoride series. According to previous studies, the combination of carbonate and fluoride components is a stable and durable species in the SEI layer.[40] The observation suggests that introducing an anthracene additive can improve the structural stability of the SEI layer formed on Li metal anodes. The O 1s spectra showed the predominant peaks of Li_2CO_3 and Li_2O_2 under all three conditions. However, in the absence of the additive, an additional ROLi peak is observed (Fig. 5d). Differences in the ROLi peaks can be observed more distinctly through depth profile analysis. Fig. S4a–S4c† reveals variations in the chemical components with etching time. In the cases without additives and with benzene, ROLi peaks were strongly formed as we moved inward. By contrast, in the presence of anthracene, only trace amounts of ROLi peaks were observed, even at deeper depths. This implies that utilizing anthracene as a highly polarizable nonpolar molecule additive suppresses the decomposition of the electrolyte solvent, preventing substan-

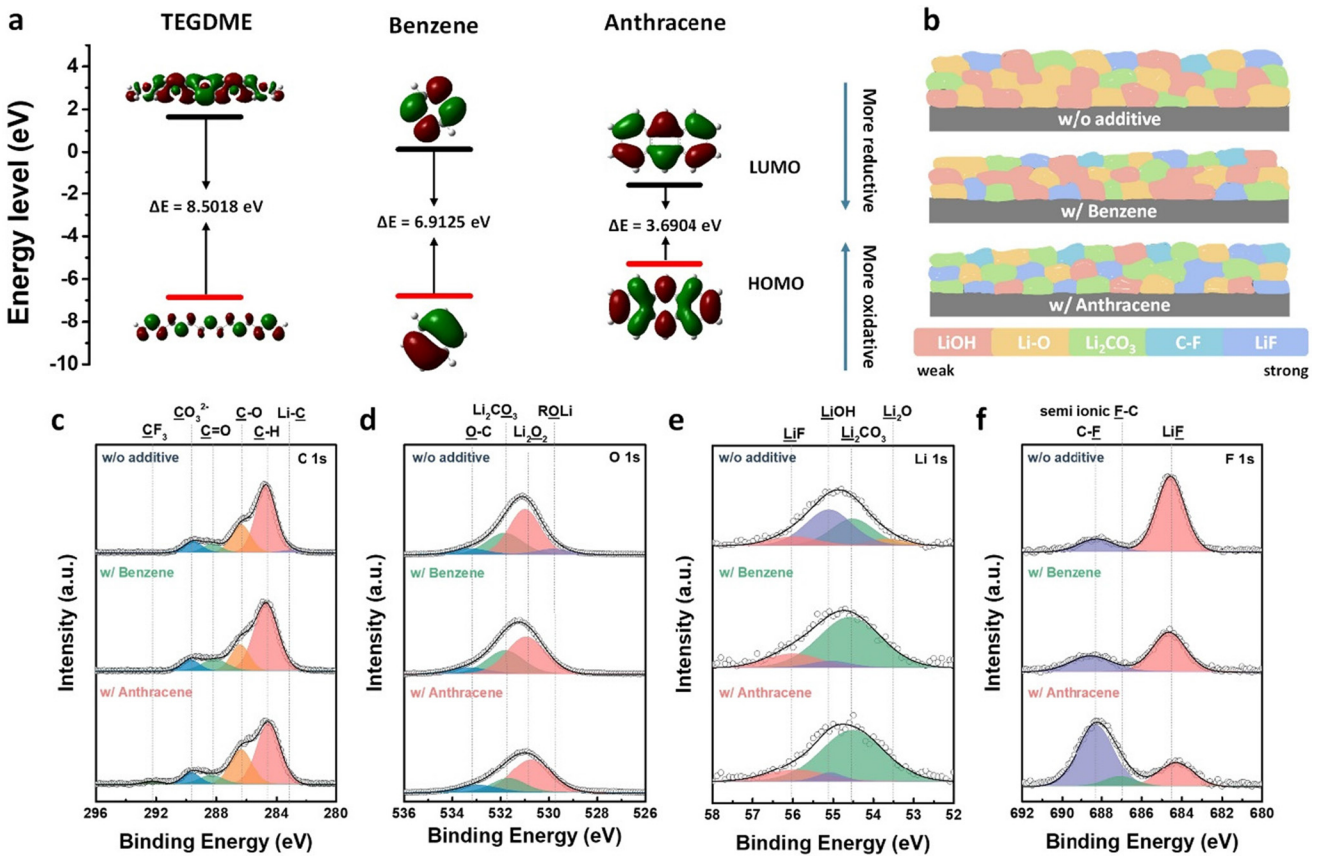

Fig. 5 (a) HOMO and LUMO energy levels of electrolyte solvent, benzene, and anthracene additive. (b) Schematic showing the composition of the SEI layer formed on the lithium metal anode surface. XPS spectra of the lithium metal anode after 30 cycles at a current density of 5 mA cm^{-2}. (c) C 1s, (d) O 1s, (e) Li 1s, and (f) F 1s spectra of the lithium metal anode cycled in the electrolyte with and without nonpolar additives.

tial electrolyte consumption. The Li 1s spectra revealed significant differences in the chemical components induced by the nonpolar additives (Fig. 5e). A strong LiOH peak and oxide components such as Li_2O were observed in the absence of additives. By contrast, when benzene and anthracene additives were introduced, durable carbonate components such as Li_2CO_3 were predominantly formed. According to previous research, an SEI layer rich in oxide components is relatively rigid and vulnerable to volume changes and mechanical stresses during repeated charge and discharge cycles, leading to continuous electrolyte consumption.[41,42] Furthermore, nonpolar additives in the electrolyte induce changes in the composition of the SEI layer, promoting the formation of a durable and flexible SEI layer with carbonate species. Finally, in the F 1s spectrum, the LiF peaks were predominant in the Li electrodes cycled without additives. By contrast, LiF and C–F peaks were observed when the benzene and anthracene additives were introduced (Fig. 5f). According to previous research, C–F components contribute positively to the formation of LiF through additional cycling.[43,44] Variations in the F 1s components in the Li electrodes cycled with different electrolyte additives are observed in the depth profile (Fig. S4d–S4f†). In the case of anthracene molecules, an SEI layer with a rich LiF component was formed internally, suggesting that this specific additive significantly enhanced the structural stability of the SEI layer. In summary, the XPS analysis demonstrated that benzene and anthracene improved the structural stability of the SEI layer through changes in its composition. This modified SEI layer can withstand severe reaction environments, such as volume changes in Li metal anodes during cycling, thereby preventing continuous electrolyte consumption and facilitating Li-ion diffusion through the beneficial SEI layer components.

3. Conclusions

In this study, we demonstrated the importance of controlling the polarizability of electrolyte additives by comparing nonpolar benzene and anthracene molecular additives with different molar volumes for longer cycling and more rapid operation of Li metal batteries. Through comprehensive experimental investigations and computational validations, we demonstrated that the polarizability of these nonpolar molecular additives, as a function of their molar volume, plays a crucial role in determining their effectiveness in stabilizing Li metal anodes. Specifically, nonpolar anthracene additives with higher polarizability exhibited superior surface stabilization effects and exceptional cycle performance compared to nonpo-

lar and lower-polarizable benzene additives. These effects include surface smoothing, control over the Li crystal growth direction, and forming a stable solid electrolyte interface layer. Moreover, our electrochemical analyses, including Li–Li symmetric cell tests and impedance spectroscopy, confirmed the significant benefits of highly polarizable and nonpolar anthracene additives in improving the battery lifespan and interfacial stability, especially under an extremely high current density of 10 mA cm^{-2} owing to the induced orbital asymmetry caused by the high applied field on the electrode surface. Surface morphology analyses further supported these findings by revealing smoother and more uniform lithium metal electrode surfaces when highly polarizable and nonpolar anthracene additives were utilized compared to the lower polarizable and nonpolar benzene additives. *Ex situ* crystalline and surface analyses revealed the positive impact of these additives on the crystalline structure and chemical composition of the SEI layer, further enhancing its structural stability and inhibiting unnecessary electrolyte decomposition. Overall, our study underscores the importance of the polarizability factor for designing electrolyte additive alternatives for ultralong and rapidly operating Li–metal batteries, thereby offering valuable insights and strategies for developing next-generation energy storage systems.

4. Experimental section

4.1. Preparation of electrolyte

Benzene (anhydrous, 99.8%), anthracene (97%), tetraethylene glycol dimethyl ether (TEGDME, 99%), and bis(trifluoromethane) sulfonimide lithium salt (LiTFSI, 99.95%) was purchased from Sigma–Aldrich (Korea). Tetraethylene glycol dimethyl ether (TEGDME, 99%) was used as the electrolyte after dipping in freshly activated 4 Å molecular sieves for two weeks. Bis(trifluoromethane) sulfonimide lithium salt (LiTFSI, 99.95%) was added to TEGDME. Benzene and anthracene were added to the electrolyte at a concentration of 1 wt%.

4.2. Preparation of Li–Li symmetric cells

A 12 mm diameter Li metal foil was used for both electrodes, and Celgard 2500 polypropylene was used as the separator. Li–Li symmetric cells were assembled using R2032 coin-type cells (Wellcos Corp.) in an argon-purged glove box. 1 M LiTFSI in TEGDME with and without 1 wt% non-polar additive was stirred for 24 h at room temperature and used as the electrolyte.

4.3. Electrochemical measurements

All electrochemical analyses were performed at room temperature. Charge/discharge tests using Li–Li symmetric cells were conducted using a battery cycler (WBCS3000S battery test system, WonATech). Electrochemical impedance spectroscopy (EIS) measurements were performed from 1 MHz to 0.01 Hz with an amplitude of 5 mV.

4.4. *Ex situ* characterization

The morphologies and surfaces of the samples were verified by field-emission scanning electron microscopy (FE-SEM, JSM-7600F, JEOL) at an accelerating voltage of 5 keV. In an argon-filled glove box, surface roughness was investigated using AFM (NX-10, Park Systems, Korea). The surface characteristics of the Li metal electrodes after cycling were investigated using X-ray photoelectron spectroscopy (XPS, K-alpha, Thermo U.K.). The crystal structure of the Li metal electrode was characterized using XRD (D8 Advance, Bruker) using Cu-Kα (λ = 1.54 Å). After charging and discharging, the cells were disassembled in an Ar-filled glove box.

Author contributions

S.-Y. J. and W.-H. R. conceived the idea and conceptualized the project. S.-Y. J., C. S., and S. K. performed the electrochemical experiments and analyzed the data. H. P. performed the electrochemical calculations and discussed the results with S.-Y. J., W.-H. R., S.-Y. J., and W.-H. R. wrote the manuscript with contributions from all the authors. W.-H. R. supervised the study. All the authors discussed the results and commented on the manuscript.

Data availability

The data that support the findings of this study are available from the corresponding author upon reasonable request. Data includes all relevant raw and processed data generated during the current study, including experimental protocols, data analysis scripts, and any ESI.† The data have been stored in a secure institutional repository and can be accessed by contacting the corresponding author at **whryu@sookmyung.ac.kr**.

Conflicts of interest

The authors declare no competing interests.

Acknowledgements

This study was supported by the National Research Foundation of Korea (NRF) grant funded by the Korean Government (MSIT) (No. RS-2023-00208983). This work was partly supported by the Korea Institute of Energy Technology Evaluation and Planning (KETEP) grant funded by the Korean government (MOTIE) (20221B1010003B, Integrated High-Quality Technology Development of Remanufacturing Spent Cathode for Low-Carbon Resource Recirculation).

References

1 F. Wu, J. Maier and Y. Yu, *Chem. Soc. Rev.*, 2020, **49**, 1569–1614.
2 X.-B. Cheng, R. Zhang, C.-Z. Zhao and Q. Zhang, *Chem. Rev.*, 2017, **117**, 10403–10473.

3 D. Lin, Y. Liu and Y. Cui, *Nat. Nanotechnol.*, 2017, **12**, 194–206.
4 F. Zheng, M. Kotobuki, S. Song, M. O. Lai and L. Lu, *J. Power Sources*, 2018, **389**, 198–213.
5 C. Sun, J. Liu, Y. Gong, D. P. Wilkinson and J. Zhang, *Nano Energy*, 2017, **33**, 363–386.
6 B. Kim, K. Shin, G. Henkelman and W.-H. Ryu, *Chem. Eng. J.*, 2023, **477**, 147141.
7 F. Peng, Y. Lim, B. Kim, H.-S. Kim, Z. Li, Z. Zhou, J. Li and W.-H. Ryu, *Sustainable Mater. Technol.*, 2023, **35**, e00531.
8 Y.-J. Rho, B. Kim, K. Shin, G. Henkelman and W.-H. Ryu, *J. Mater. Chem. A*, 2022, **10**, 19710–19721.
9 H. S. Kim, B. Kim, H. Park, J. Kim and W. H. Ryu, *Adv. Energy Mater.*, 2022, **12**, 2103527.
10 J.-S. Lee, K. Shin, S.-Y. Jun, S. Kim and W.-H. Ryu, *Chem. Eng. J.*, 2023, **458**, 141383.
11 S. Y. Jun, K. Shin, J. S. Lee, S. Kim, J. Chun and W. H. Ryu, *Adv. Sci.*, 2023, **10**, 2301426.
12 X. Zhang, A. Wang, X. Liu and J. Luo, *Acc. Chem. Res.*, 2019, **52**, 3223–3232.
13 L. Ma, J. Cui, S. Yao, X. Liu, Y. Luo, X. Shen and J.-K. Kim, *Energy Storage Mater.*, 2020, **27**, 522–554.
14 X. B. Cheng, R. Zhang, C. Z. Zhao, F. Wei, J. G. Zhang and Q. Zhang, *Adv. Sci.*, 2016, **3**, 1500213.
15 X.-R. Chen, C. Yan, J.-F. Ding, H.-J. Peng and Q. Zhang, *J. Energy Chem.*, 2021, **62**, 289–294.
16 R. Zhang, X. Shen, Y.-T. Zhang, X.-L. Zhong, H.-T. Ju, T.-X. Huang, X. Chen, J.-D. Zhang and J.-Q. Huang, *J. Energy Chem.*, 2022, **71**, 29–35.
17 N. W. Li, Y. Shi, Y. X. Yin, X. X. Zeng, J. Y. Li, C. J. Li, L. J. Wan, R. Wen and Y. G. Guo, *Angew. Chem.*, 2018, **130**, 1521–1525.
18 N. W. Li, Y. X. Yin, C. P. Yang and Y. G. Guo, *Adv. Mater.*, 2016, **28**, 1853–1858.
19 T. Zhang, X. Li, X. Miao, R. Sun, J. Li, Z. Zhang, R. Wang, C. Wang, Z. Li and L. Yin, *ACS Appl. Mater. Interfaces*, 2022, **14**, 14264–14273.
20 X. Li, L. Yuan, D. Liu, M. Liao, J. Chen, K. Yuan, J. Xiang, Z. Li and Y. Huang, *Adv. Funct. Mater.*, 2021, **31**, 2100537.
21 W. Ren, Y. Zheng, Z. Cui, Y. Tao, B. Li and W. Wang, *Energy Storage Mater.*, 2021, **35**, 157–168.
22 L. Shen, X. Liu, J. Dong, Y. Zhang, C. Xu, C. Lai and S. Zhang, *J. Energy Chem.*, 2021, **52**, 262–268.
23 R. Pan, X. Xu, R. Sun, Z. Wang, J. Lindh, K. Edström, M. Strømme and L. Nyholm, *Small*, 2018, **14**, 1704371.
24 C. Chen, Q. Liang, G. Wang, D. Liu and X. Xiong, *Adv. Funct. Mater.*, 2022, **32**, 2107249.
25 D. Kang, M. Xiao and J. P. Lemmon, *Batteries Supercaps*, 2021, **4**, 445–455.
26 Y. Liu, R. Hu, D. Zhang, J. Liu, F. Liu, J. Cui, Z. Lin, J. Wu and M. Zhu, *Adv. Mater.*, 2021, **33**, 2004711.
27 S. Li, Z. Luo, L. Li, J. Hu, G. Zou, H. Hou and X. Ji, *Energy Storage Mater.*, 2020, **32**, 306–319.
28 H. Zhang, G. G. Eshetu, X. Judez, C. Li, L. M. Rodriguez-Martínez and M. Armand, *Angew. Chem., Int. Ed.*, 2018, **57**, 15002–15027.
29 S. Li, W. Zhang, Q. Wu, L. Fan, X. Wang, X. Wang, Z. Shen, Y. He and Y. Lu, *Angew. Chem., Int. Ed.*, 2020, **59**, 14935–14941.
30 X. Li, J. Zheng, X. Ren, M. H. Engelhard, W. Zhao, Q. Li, J. G. Zhang and W. Xu, *Adv. Energy Mater.*, 2018, **8**, 1703022.
31 N. Piao, S. Liu, B. Zhang, X. Ji, X. Fan, L. Wang, P.-F. Wang, T. Jin, S.-C. Liou and H. Yang, *ACS Energy Lett.*, 2021, **6**, 1839–1848.
32 S. Y. Jun, K. Shin, Y. Lim, S. Kim, H. Kim, C. Y. Son and W. H. Ryu, *Small Struct.*, 2024, 2300578.
33 S. Menkin, J. B. Fritzke, R. Larner, C. de Leeuw, Y. Choi, A. B. Gunnarsdóttir and C. P. Grey, *Faraday Discuss.*, 2024, **248**, 277–297.
34 J.-J. Woo, V. A. Maroni, G. Liu, J. T. Vaughey, D. J. Gosztola, K. Amine and Z. Zhang, *J. Electrochem. Soc.*, 2014, **161**, A827.
35 W. Waag, S. Käbitz and D. U. Sauer, *Appl. Energy*, 2013, **102**, 885–897.
36 A. Keefe, S. Buteau, I. Hill and J. Dahn, *J. Electrochem. Soc.*, 2019, **166**, A3272–A3279.
37 C. Chen, J. Liu and K. Amine, *J. Power Sources*, 2001, **96**, 321–328.
38 Q. Zhao, Y. Deng, N. W. Utomo, J. Zheng, P. Biswal, J. Yin and L. A. Archer, *Nat. Commun.*, 2021, **12**, 6034.
39 F. Shi, A. Pei, A. Vailionis, J. Xie, B. Liu, J. Zhao, Y. Gong and Y. Cui, *Proc. Natl. Acad. Sci. U. S. A.*, 2017, **114**, 12138–12143.
40 M. He, R. Guo, G. M. Hobold, H. Gao and B. M. Gallant, *Proc. Natl. Acad. Sci. U. S. A.*, 2020, **117**, 73–79.
41 E. Peled and S. Menkin, *J. Electrochem. Soc.*, 2017, **164**, A1703.
42 J. E. Owejan, J. P. Owejan, S. C. DeCaluwe and J. A. Dura, *Chem. Mater.*, 2012, **24**, 2133–2140.
43 X. Q. Zhang, X. B. Cheng, X. Chen, C. Yan and Q. Zhang, *Adv. Funct. Mater.*, 2017, **27**, 1605989.
44 H. Shin, J. Park, A. M. Sastry and W. Lu, *J. Electrochem. Soc.*, 2015, **162**, A1683.